Measurement of the Branching Ratios of $K_{\mu 2}^+$, $K_{\pi 2}^+$, K_{e3}^+, and $K_{\mu 3}^+$†

L. B. AUERBACH, J. MACG. DOBBS,* A. K. MANN, W. K. MCFARLANE, AND D. H. WHITE‡
University of Pennsylvania, Philadelphia, Pennsylvania

AND

R. CESTER,§ P. T. ESCHSTRUTH, G. K. O'NEILL, AND D. YOUNT‖
Princeton University, Princeton, New Jersey

(Received 7 September 1966)

In an experiment performed at the Princeton-Pennsylvania Accelerator with scintillation counters and spark chambers, we have determined the branching ratios for the K^+ decay modes $K_{\mu 2}^+$, $K_{\pi 2}^+$, $K_{\mu 3}^+$, and K_{e3}^+. For each event, we measured the momentum and range of the charged secondary and the time interval between the arrival of the K^+ and its decay. The momentum was measured in thin-foil spark chambers placed in a magnetic field. The range was then measured in a thick-plate spark chamber in which all charged products from K^+ decay were stopped. K^+ decays in flight were eliminated through use of the timing information. The solid angle and detection efficiency of the apparatus were constant over the momentum interval 130 to 260 MeV/c. Based on approximately 23 000 measured events, our values for the branching ratios are (63.34±0.44)% for $K_{\mu 2}^+$, (20.59±0.40)% for $K_{\pi 2}^+$, (4.97±0.16)% for K_{e3}^+, and (3.82±0.29)% for $K_{\mu 3}^+$. These values have been determined by using for the τ and τ' branching ratios (5.58±0.08)% and (1.70±0.055)%, respectively. A table of weighted averages of all K^+ branching-ratio measurements is included.

I. INTRODUCTION

ALL present values of the K^+ branching ratios have been obtained from emulsion and bubble-chamber experiments. The emulsion experiments were pioneer ones, generally with poor statistics, and the separation of modes involving particles with momentum greater than about 170 MeV/c was usually done with ionization and multiple-scattering measurements, which are sometimes ambiguous in their application to particles in that mass and momentum region. The bubble-chamber experiments are generally satisfactory statistically but the particle-detection efficiency is mode and momentum dependent and hence relatively elaborate event-weighting procedures have been required. In most instances, corrections due to the overlapping of products from different decay modes and to the presence of undetected K^+ and π^+ decays in flight are not negligible and require a sophisticated analysis to obtain a meaningful result. A summary of the experimental situation (see Table II, Sec. V) indicates that certain of the branching-ratio values, particularly for $K_{\mu 3}^+$ and $K_{\pi 2}^+$, are in disagreement by two or more standard deviations, presumably indicating the presence of systematic effects which have not been accounted for. On the other hand, the branching ratios of the decay modes $K^+ \to \pi^+ + \pi^+ + \pi^-$ (τ) and $K^+ \to \pi^+ + \pi^0 + \pi^0$ (τ') have been measured in a number of closely agreeing experiments using bubble chambers (see Appendix A), which have advantages over other experimental methods in the measurement of decay modes with low-momentum product particles and relatively clear signatures.

In this paper we report on two spark-chamber experiments in which the branching ratios $K_{\mu 2}^+$, $K_{\pi 2}^+$, $K_{\mu 3}^+$, and K_{e3}^+ were determined. The spark chamber-counter technique as applied here directly measured the momentum of the charged particle from a particular decay mode by observing its trajectory in a spark chamber in a magnetic field. In one experiment, the momentum chamber was followed by a threshold gas Čherenkov counter to identify positrons. In a second experiment, the momentum chamber was followed by another spark chamber to identify muons and pions by range measurement; in this experiment electrons were also detected by having measured ranges not appropriate to either muons or pions. With these experimental arrangements, overlapping of the various decay modes was minimized and the detection efficiencies were quite high for all modes and uniform over wide intervals of momentum. K^+ decays in flight were eliminated by measuring the decay time of each event. The geometry of the apparatus and the thickness of material involved set lower limits on the momenta of particles that were measurable in these experiments and made unobservable most charged particles from the decay modes τ and τ'.

The experiment on the positron momentum distribution and branching ratio of K_{e3}^+ that used a gas Čherenkov counter involved a different normalization procedure and a different method of positron identification than the experiment that used a range spark chamber. The former experiment has been briefly described in an earlier publication.[1] It is included here, although the experiments were done independently, to provide a few additional experimental details concerning it and to

† Work performed under the auspices of the Atomic Energy Commission.

* Present address: Washington University, St. Louis, Missouri.
‡ Present address: Cornell University, Ithaca, New York.
§ Present address: Istituto di Fisica, Universita di Torino, Torino, Italy.
‖ Present address: Stanford Linear Accelerator Center, Stanford, California.

[1] R. Cester, J. MacG. Dobbs, P. T. Eschstruth, A. K. Mann, W. K. McFarlane, G. K. O'Neill, B. Quassiatti, D. H. White, and D. Yount, Phys. Letters **21**, 343 (1966). Note that the error quoted in this paper on the ratio of rates $K_{e3}/(K_{\pi 2}+K_{\mu 2})$ is wrong and this ratio should be (0.0589±0.0021).

emphasize the complementary nature of the two measurements.

II. EXPERIMENTAL ARRANGEMENT

A positive unseparated beam was obtained with the beam transport system shown in Fig. 1. The circulating proton beam of the Princeton-Pennsylvania Accelerator (PPA) struck an internal platinum target at a mean energy of about 2.8 BeV. Particles leaving the target at a mean angle of 46° to the primary beam were brought to a first focus just beyond the bending magnet, by the first pair of quadrupoles. The second doublet then focused this image on to the K^+ detection apparatus. This double focusing system had a wide momentum bite (7% FWHM, full width at half maximum) without producing a large spatial dispersion at the final focus. The beam was bent in the off-axis quadrupoles to discriminate against fast proton backgrounds and to provide control of the beam position. The central momentum was 525 MeV/c, with an over-all length (target-to-final focus) of 8.8 m, and the solid angle subtended at the target for the central momentum was 4.5×10^{-3} sr.

The beam entering the K^+ detection system was composed of protons and pions in the ratio 2:1, with a small number of muons, positrons, and kaons. The pion-to-kaon ratio was about 300:1. The counter system used to identify the stopping K^+ mesons is shown in Fig. 2.

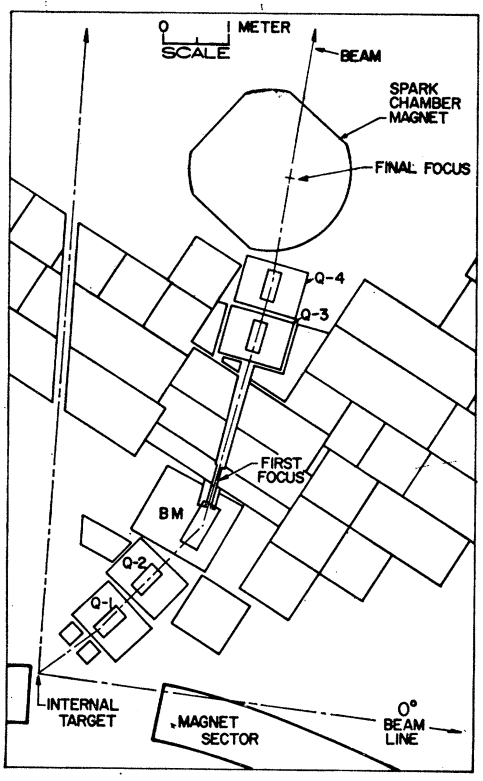

FIG. 1. Layout of the 525-MeV/c positive unseparated beam.

Counter C_3 was the stopping region and was 2.5-cm wide, 5-cm high, and 10 cm along the beam. Enough copper (7.0 cm) was put in front of C_2, the beam counter, to stop most kaons in C_3. This amount of copper was sufficient to remove almost all protons from the beam. Particles that did not stop or scatter in C_3 were vetoed by counter C_4. About 75% of the pions passed through C_4.

The kaons were identified, apart from the above range measurement, by time of flight. The internal beam of the PPA retains its bunched structure and phase relative to the driving radio-frequency waveform when it strikes the internal target. The proton bunches are less than 1.5 nsec wide and 34 nsec apart and the

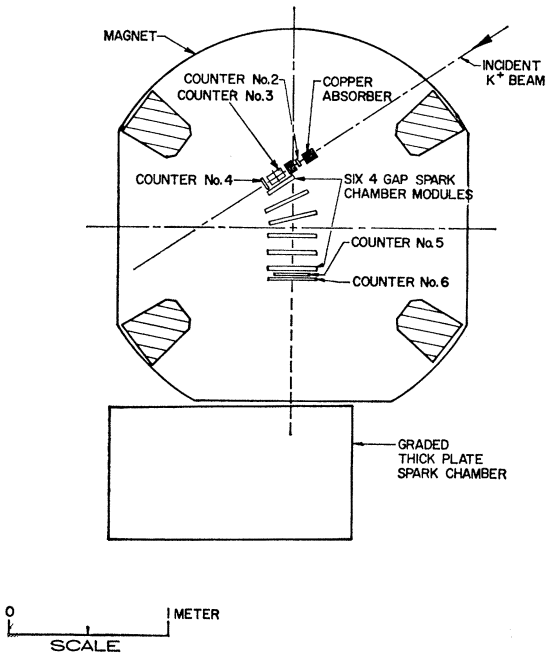

FIG. 2. Plan view of the experimental setup using the range measuring chamber. A plan of the apparatus with the Čherenkov counter in place may be seen in Ref. 1.

signal derived from the synchrotron rf system may be used as a time mark (with ambiguities of multiples of 34 nsec) to measure times of flight, over the full length of the beam. The time separation between π's and K's was about 10 nsec, providing adequate discrimination with a 4-nsec wide coincidence between C_2 and a discriminator C_1 triggered by the rf master oscillator of the synchrotron. By continuous monitoring of the relative time of the C_1 signal and the majority of signals (i.e., pions) from C_2, the (C_1C_2) coincidence was kept correctly adjusted for kaons, despite small variations in the phase of the master oscillator relative to the circulating beam bunches. Only about one-fifth of the rf "buckets" contained a pion, so that only this fraction of K's was lost due to being preceded by a pion from

the same primary bunch. The counting rate of ($C_1C_2C_3\bar{C}_4 = A_1$) coincidences as a function of the relative delay of C_1 is shown in Fig. 3, where it is seen that when the timing is set for K^+ the π^+ background is only about 5% of the K^+ rate. The over-all momentum acceptance of the beam and counter system was about 4% FWHM, with an average rate of about 200 stopped, identified kaons per second.

Passage of decay products through the spark chambers was detected by the coincidence telescope C_5 and C_6 at the exit of the momentum spark chamber. A 20-nsec pulse generated by A_1 coincidences was placed in

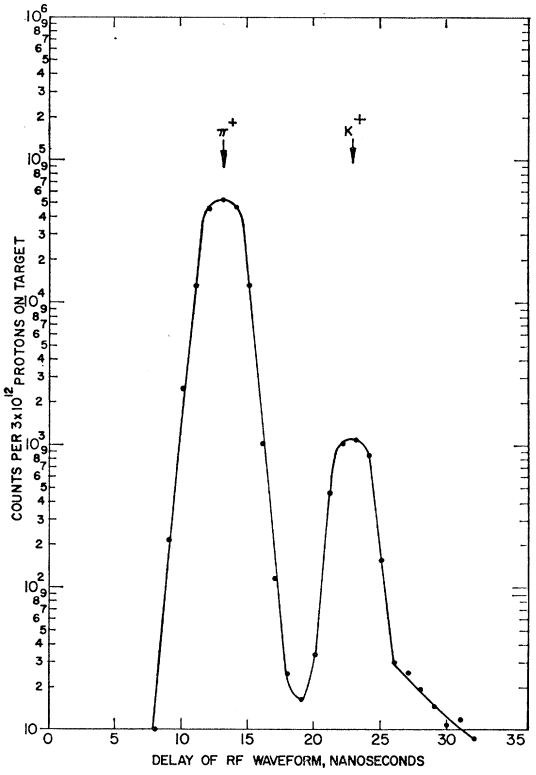

FIG. 3. Observed K^+ stopping rate as a function of delay of the synchrotron master oscillator waveform.

coincidence with C_5 and C_6 to allow the detection of K^+ decays from prompt time to about 1.7 K^+ lifetimes. The gate was cut off at 21 nsec to avoid background from pions in the succeeding rf bucket. The spectrum of the time interval between the C_3 and (C_5C_6) pulses, gated by ($A_1C_5C_6 = A_2$) coincidences, shows in Fig. 4 a prompt peak from K^+ decays in flight and charge exchange interactions, followed by an exponential decay with the K^+ lifetime. As shown in Fig. 4, background due to random A_2 coincidences amounted to about 10% of the rate.

The momentum chamber was oriented relative to the stopping region so that on average the lowest momentum secondaries left the stopping region at right angles

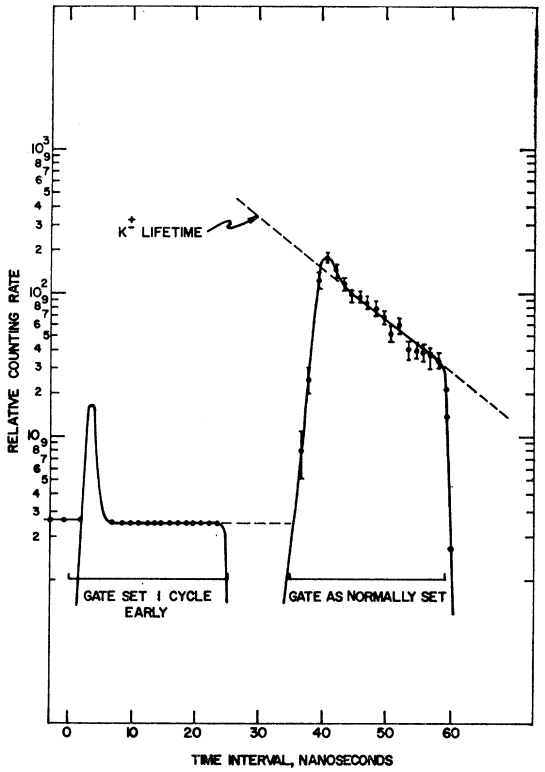

FIG. 4. Time spectrum of normal triggers and of accidentals. Normally, the gate was generated by an A_1 coincidence and extended 21 nsec later than A_1. For accidentals, the gate was shifted to start one rf cycle earlier than A_1.

to the beam, thus minimizing energy loss. In order to achieve the maximum chord length and a momentum-independent solid angle, the target was placed on one corner of the viewable region. The magnetic field was vertical and occupied a 60-cm-diameter circular region about 35 cm high. A rectangular area 30×60 cm was viewed along the field direction, through a hole in the upper pole piece. The magnetic field, which varied by a total of about 30% over the useful volume, was mapped to a relative precision of 0.2%, at points separated by 2.5 cm on a three-dimensional rectangular lattice. The number of chambers and gaps was chosen to optimize the resolution over the selected momentum range, and was a compromise between the number of measurements (with all sparks measured) and multiple scattering in the foils. Six spark chambers were placed between the stopper C_3, and the end of the viewable region. All had a sensitive area 30 cm wide and 25 cm high except the first which was 17.5 cm wide and 12.5 cm high. The first three chambers were fanned out to reduce the average angle between the normal to the plates and the tracks. Each chamber had four gaps, with a total aluminum thickness of 30 mg/cm^2. To reduce the memory time of the chamber, the basic 90% Ne, 10% He mixture was poisoned with about 0.2% of sulphur dioxide.

The accuracy of the momentum measurement at a given field was affected by random spark scatter, multiple scattering in the chamber, optical distortions and field-measurement errors. Only the first two effects were important. Using the measured spark scatter, the expected momentum resolution at 5 kG was calculated to vary from 2.5% (standard deviation) at 100 MeV/c to 2.1% at 250 MeV/c. The momentum resolution obtained (1.8% at 235 MeV/c) with $K_{\mu 2}^+$ events is shown in Fig. 8(a).

The angular acceptances of the detection devices that followed the momentum chamber were made appropriate to the output of that chamber in order to provide uniform detection efficiency. For each magnetic field, it was possible to achieve this over certain intervals of momentum. This was verified by comparison of momentum and spatial distributions of observed events with Monte Carlo generated events. Within these momentum intervals the solid angle was defined by the horizontal acceptance of C_5 and by the vertical acceptance of the magnet and was 0.8% of the sphere.

The range chamber had 42 plates of graded thickness, and was designed to provide separation of pions and muons. The thicknesses were so chosen that a pion and muon of the same momentum differed in range by about five chamber gaps. This also had the result that each plate thickness was about equal to the theoretical range straggling for a particle stopping at that plate. Plates were of aluminum or magnesium and varied in thickness from 0.56 g/cm^2 at the beginning of the chamber to 3.5 g/cm^2 at the end. The total thickness was 80 g/cm^2, and the dimensions large enough (137 cm$\times$60 cm) to accept all particles in the required momentum range. The thickness of material in front of the first gap of the range chamber was sufficient to make 120 MeV/c the lower limit for detection of muons with full efficiency.

The gas Čherenkov counter and the method of its employment in the K_{e3}^+ measurements have been previously described.[1,2] The measured efficiency of the counter for positrons in the desired angular range was 97$\pm$1% and for other particles about 0.7%.

The last-dynode outputs of C_3 and C_5 were mixed and displayed on a 20-nsec/cm oscilloscope trace, triggered by the fast pulse which also triggered the spark chambers. The measured time interval between the C_3 and C_5 pulses permitted the complete elimination of K^+ decays in flight by selection of events for which the C_5 pulse came at least 2.5 nsec later than prompt C_5 pulses.

The data for each event were recorded on 35-mm film using two cameras. The spark chamber used four full frames: a parameter frame, two frames giving two views of the momentum chamber in 90° stereo, and one frame giving two views of the range chamber in 90° stereo. The oscilloscope camera recorded the time trace on a single frame.

[2] J. MacG. Dobbs, W. K. McFarlane, and D. Yount, Nucl. Instr. Methods (to be published).

III. DATA REDUCTION

All the film was scanned twice and 25% of it was scanned a third time. The scanning efficiency after double scanning was 97$\pm$1%. The third scan was used to check for systematic variations in scanning criteria. In the momentum interval 100 to 260 MeV/c, the scanning efficiency was found to be independent of decay mode and particle momentum, and there were no systematic variations in scanning criteria.

An event was measured if it had one and only one measurable track in each chamber. In the momentum chamber a measurable track was defined as one spark or more in each module. Every spark along a momentum chamber track was measured. When events were computed, only those which had at least 18 matched sparks were accepted. Every scope trace was measured, provided it showed two clearly separated pulses in appropriate time sequence. The measurement procedure defined the base line of the trace and the leading edge and height of each pulse.

In the range chamber, a measurable track was required to exhibit at least three sparks and to start at the beginning of the chamber. Only the first spark, the last spark, and a spark at each visible scattering were measured. It was found that $K_{\mu 2}^+$ events were easily recognized during scanning by their characteristic range. The tracks that stopped in the 36th, 37th, or 38th plate of the range chamber were entirely from $K_{\mu 2}^+$, and comprised about half of all $K_{\mu 2}^+$ events. In order to save measuring time these events were recorded (providing they satisfied all other measuring requirements) by measuring only the first and last sparks of the range-chamber tracks, and the time trace. In order to combine the "scanned $K_{\mu 2}^+$ events" with the "measured" events, about 20% of the film was measured without using the time-saving procedure, all measurable events being fully measured.

To calculate the momentum, the measured points were corrected for optical distortions and spark shifting and then fitted to polynomials, third order in the top view, second order in the side view. The momentum was computed for each of 30 points along the track using the curvature of the polynomial and the value of the magnetic field at the particular point. The momentum for each event was taken to be the weighted average of these momenta. A reconstructed track with this momentum was generated using the position and direction of the measured track at its midpoint. This track was projected through the K^+ stopping region and the range chamber or gas Čherenkov counter.

To obtain the range, the range chamber track was reconstructed as a series of straight-line segments. The thickness of each plate crossed by the track was multiplied by the appropriate angular correction and the thicknesses summed. It was assumed in this sum that the track ended halfway through the plate beyond the last spark of the measured track.

The decay time was computed from the time difference between the intersection of the leading edge of each pulse on the scope trace with the base line. Since the momentum distribution of the $K_{\mu 2}^+$ events from K^+ decays in flight overlaps the $K_{\mu 3}^+$ distribution, it was important to make sure that the K^+ had come to rest before decaying.

Events that were accepted as satisfactory after computation were required to satisfy the following six criteria: (1) The decay time of the event was greater than 2.5 nsec; (2) the spatial coordinates of the projected track were in the K^+ stopping region; (3) the projected track passed through counters 5 and 6; (4) the projected track traversed a given area at the front of the range chamber; (5) in the momentum chamber, the standard deviation of the sparks from the fitted polynomial was less than 0.065 cm in each view; (6) it was required that the projection of the momentum-chamber track correspond to the observed range-chamber track at the first plate of the range chamber, within limits set by multiple scattering and uncertainties in the track fitting. The event distributions for items (5) and (6) are shown in Figs. 5 and 6, respectively. The momentum independence of the selection criteria was verified by comparing the shapes of various distributions such as those in Fig. 5 and 6 for different momentum intervals.

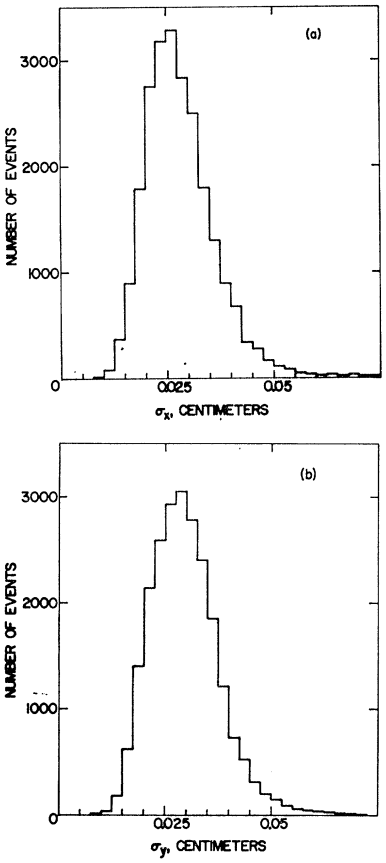

FIG. 5. Distribution of the standard deviation σ of the sparks from the calculated trajectory: (a) top (x) view and (b) side (y) view.

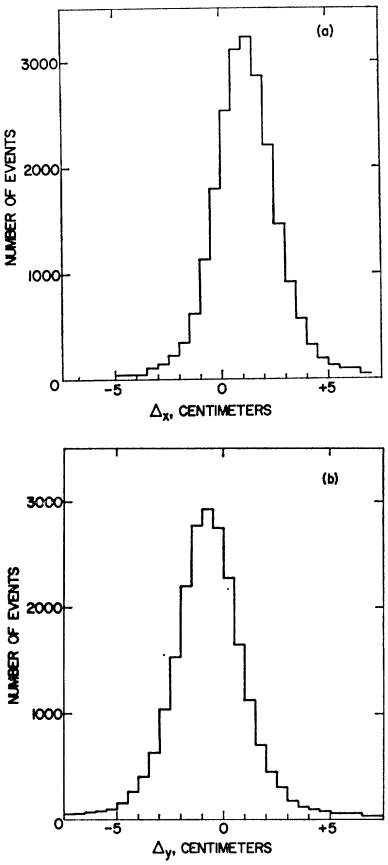

FIG. 6. Distribution of the difference Δ of the observed coordinates of the K^+ secondary entering the range chamber from those predicted by extrapolating the momentum-chamber track: (a) x view and (b) y view.

The data obtained in the experiment that employed the gas Čherenkov counter were treated as described above, with the exceptions that: (a) No time selection criterion was necessary since the K_{e3}^+ sample was not contaminated by other decay modes and since the spectrum shape for K_{e3}^+ was, within statistics, unaffected by the decays in flight; (b) criterion (4) was replaced with the requirement that the projected track traverse a given area at the back of the Čherenkov counter to insure that it was in the uniformly efficient region of that counter; and (c) criterion (6) was omitted, since there was no range chamber.

IV. RESULTS

A. $K^+ \rightarrow \mu^+ + \nu$

Figure 7 is a range-momentum scatter plot of all the measured events which satisfied the selection criteria, including the decay-time cut at 2.5 nsec. There are 11 214 events in this plot, all obtained with a nominal magnetic field of 5 kG applied to the momentum chamber. The decay modes $K_{\mu 2}^+$, $K_{\pi 2}^+$, K_{e3}^+, and $K_{\mu 3}^+$ are clearly discernible. At the momentum of the π^+ from $K_{\pi 2}^+$ at 205 MeV/c, one sees particles of varying range, due in part to pion-nucleus interactions in the aluminum

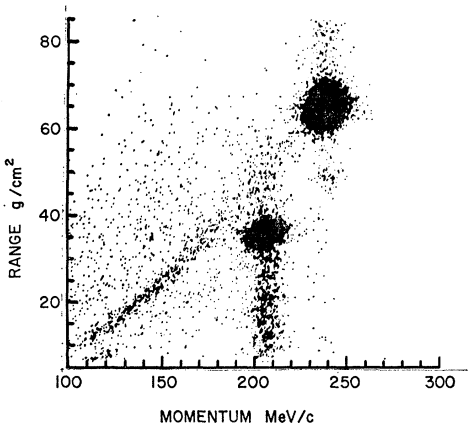

FIG. 7. Scatter plot of momentum versus range for all measured events which had decay times greater than 2.5 nsec and passed the spatial selection criteria.

and in part to muons from pions which have decayed in flight.

There were 6510 events in our measured $K_{\mu 2}^+$ sample which satisfies all the selection criteria, and were in the momentum interval from 220 to 260 MeV/c. With our momentum resolution, the number of $K_{\mu 2}^+$ events outside this interval, as well as the number of $K_{\mu 3}^+$, K_{e3}^+, and $K_{\pi 2}^+$ inside was negligible. In addition to the measured sample, there were 9389 "scanned $K_{\mu 2}^+$ events" with decay times greater than 2.5 nsec. Before combining the events in these two classes corrections were necessary to account for difference in event loss from the two samples. The correction factors were: (a) 0.938±0.002 for losses in computed events due to measurer errors, too few matching sparks in the two views of the momentum chamber, etc., (b) 0.988±0.001 for bookkeeping and card-handling losses, and (c) 0.836 ±0.002 for event loss due to the application of the six selection criteria mentioned above. Applying these factors to the scanned sample yielded 7275 events which when combined with the measured sample gives a total of 13 785 events. Adding (58±30) events to account for radiative decays[3] ($K_{\mu\nu\gamma}$) outside the momentum interval, we obtain a final number of 13 843±132 $K_{\mu 2}^+$ events (including $K_{\mu\nu\gamma}$). The momentum and range distributions of all events are given in Figs. 8(a) and 8(b). The "scanned $K_{\mu 2}^+$ events" have been included using the measured momentum and range distributions appropriate to them.

B. $K^+ \rightarrow \pi^+ + \pi^0$

The number of $K_{\pi 2}^+$ events is obtained by taking all the events in the $K_{\pi 2}^+$ momentum interval, that is, from 190 to 220 MeV/c, subtracting from them the contributions expected from the K_{e3}^+, $K_{\mu 3}^+$, and $K_{\mu\nu\gamma}^+$ decay modes, and then correcting for losses due to nuclear scattering and absorption of π^+ in the K^+ stopping counter (C_3), and for absorption in C_5, C_6, and the first three plates of the range chamber. We also apply a correction for event loss due to pion decays in flight in the momentum chamber.

There were 4195 events in the $K_{\pi 2}^+$ raw sample. From this, we subtracted 156±11 events to account for the background from $K_{\mu 3}^+$, K_{e3}^+, and $K_{\mu\nu\gamma}^+$ modes. Using a mass distribution of events with $p \leq 190$ MeV/c we found that there were 66±16 pions scattered in C_3 into the momentum interval 110 to 190 MeV/c. Pions that were scattered in C_3, C_5, and C_6 to momenta less than 110 MeV/c and those absorbed in the first three plates of the range chamber did not produce range-chamber tracks. From the observed attenuation of pions past the third plate of the range chamber, we calculated the number of pions scattered and absorbed in the material preceding the range chamber and in the first three plates of the range chamber to be 216±30. Finally, from a Monte Carlo calculation of pion decays in flight, we found that (4.0±0.3)% of all π's would be lost. Applying all the corrections given above, the final number of $K_{\pi 2}^+$ events was 4501±80.

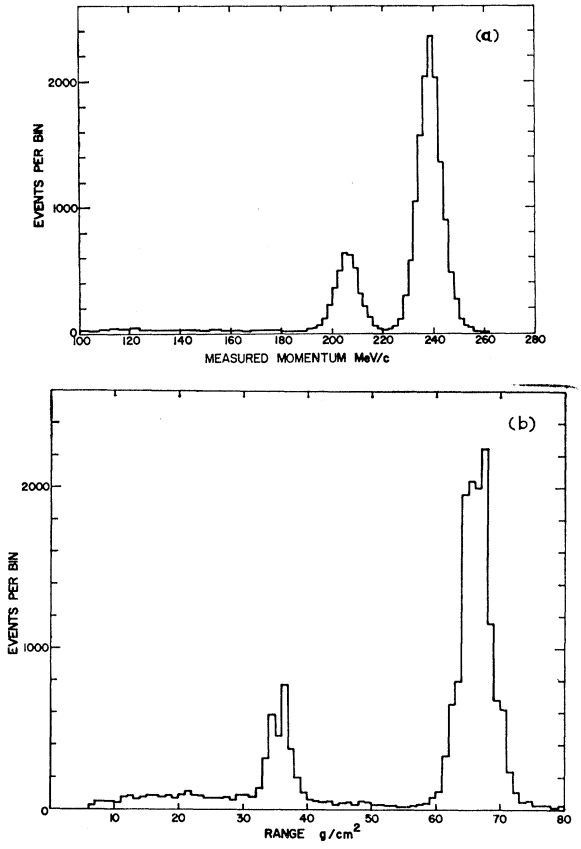

FIG. 8. (a) Momentum distribution and (b) range distribution of all events in the data sample including the scanned $K_{\mu 2}$ events which have been incorporated using the appropriate range and momentum distribution.

[3] See for example N. Cabibbo, Nuovo Cimento 11, 827 (1959); and E. Ginsberg, Phys. Rev. 142, 1035 (1966).

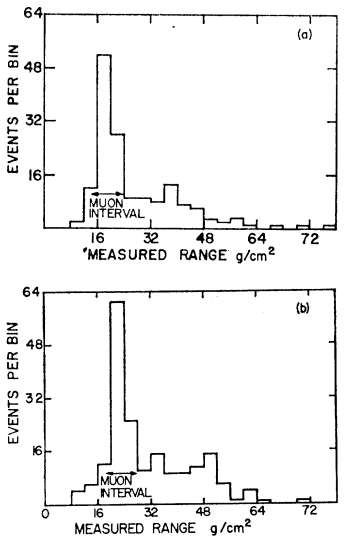

FIG. 9. The range distribution of particles in the momentum intervals (a) 130–140 MeV/c and (b) 140–150 MeV/c.

C. $K^+ \rightarrow \pi^0 + e^+ + \nu$

To separate the K_{e3}^+ and $K_{\mu 3}^+$ modes, a series of range distributions was plotted for 10 MeV/c momentum intervals from 130 to 190 MeV/c. Two of these distributions are shown in Fig. 9. For each momentum interval, a range interval was chosen which safely contained all the muons. There were 393 events outside these range-momentum intervals, of which we estimated that 45±12 were scattered pions from $K_{\pi 2}^+$ and the rest positrons. To calculate the number of positrons in the muon region, we used data from a separate run in which the wide-angle gas Cherenkov counter was placed between the momentum and range chambers so that only positrons would trigger the system. Range distributions were obtained for 2760 events in the momentum intervals 130 to 160 MeV/c and 160 to 190 MeV/c. By combining these range distributions with the momentum distribution for positrons, we formed the density function $\rho(R,p)=d^2N/dRdp$ normalized so that

$$\int_0^{R_{\max}} \int_{130}^{190} \rho(R,p)dRdp = 1.$$

Taking the integral (which we call I_μ) of $\rho(R,p)$ over the muon range-momentum region, we obtained, for the total number of positrons in the interval 130 to 190 MeV/c, $348/(1-I_\mu)=472\pm31$. In order to obtain this number without making a pion subtraction, the "muon" range intervals were widened to include both muons and pions. Evaluating $I_{\mu+\pi}$, we obtained, for 295 events outside this region, $295/(1-I_{\mu+\pi})=478\pm30$ events. We took a weighted average of 474.8±30. This number was corrected down by 1% to account for positrons from muon decays giving as the final observed number 472 ± 30 K_{e3}^+ events. The corrections for losses due to bremsstrahlung and Daltiz pairs and gain due to γ conversion were equal in magnitude for the momentum interval 130 to 190 MeV/c. The total number, over the entire K_{e3}^+ spectrum, was then 1103±74 events, where we have assumed a vector spectrum with constant form factor.

D. $K^+ \rightarrow \pi^0 + \mu^+ + \nu$

There were 456 events in the muon region of the range-momentum intervals. From this number we subtracted 118.6±7.5 events to eliminate positrons, 20.4±10 events to correct for $K_{\mu\nu\gamma}^+$ and 11.4±1.0 events to correct for pion decays in flight. The pion decay in flight subtraction was done with a Monte-Carlo calculation. The 305.6 events remaining were corrected upward by 1.3% to account for muon decay, giving 309.6±24 as the final observed number of $K_{\mu 3}^+$ events between 130 and 190 MeV/c.

E. Background

The principal backgrounds (i.e., events not from K^+ decay at rest) were of the following five types:

(1) K^+ decays in flight.
(2) K^+ charge exchange in C_3 followed by K^0 decay.
(3) Beam particles which trigger the system, by having a time of flight appropriate to a K^+, and scatter into the solid angle of the detector.
(4) Stopping K^+ which do not decay into the detector, followed by beam particles which scatter into both spark chambers.
(5) K^+ which have a decay product in the solid angle of the momentum chamber, but where the range-chamber track is from some other source.

Backgrounds (1), (2), and (3) made up about 5% of the triggers, and all gave "prompt" events which could therefore be eliminated by the time-of-decay requirement. Note from Fig. 3 that the selection of K^+ is very good. By looking at the time spectrum of events which are not expected to be from K^+ decay (i.e., particles with momentum greater than 270 MeV/c and muons with momentum between 215 and 225 MeV/c) a time-of-decay requirement was fixed, which eliminated all prompt events within the precision of the experiment. It was found that the final branching ratios were independent of reasonable variations of this requirement.

Background of type (4) is expected to be low since the time structure of the beam gives a period of 20 nsec after the arrival of each K^+ in which the beam intensity is very low (see Figs. 3 and 4). We would expect that this background would consist mostly of pions, positrons, and protons. Looking in regions where K^+ decay gives few particles we see very few (less than 15) events which cannot be associated with K^+ decay. Note that the cluster of events at the $K_{\mu 2}^+$ momentum but with shorter range are due to spark-chamber malfunctions; these constitute less than 1% of the total number of $K_{\mu 2}^+$ events. In order to discriminate against

backgrounds of type (5) we select only events where the momentum-chamber track extrapolates into the solid angle of the range chamber, and the momentum is high enough (above 130 MeV/c) that the particle would unquestionably have a measurable track in the range chamber. By looking at events in which the matching between the range chamber and extrapolated momentum-chamber tracks is poor, we estimate a total background contribution of two events from this type.

We therefore conclude that all backgrounds in our selected event sample are negligible.

F. Rates Relative to $K_{\mu 2}^+$ and Branching Ratios

The relative rate $K_{\pi 2}^+/K_{\mu 2}^+$, obtained directly from the numbers given above, is $K_{\pi 2}^+/K_{\mu 2}^+=0.3253\pm0.0065$. Similarly, for K_{e3}^+ we get $K_{e3}^+/K_{\mu 2}^+=0.0797\pm0.0054$. In the experiment in which the Cherenkov counter was used in place of the range chamber, we measured the relative rate $K_{e3}^+/(K_{\pi 2}^+ + K_{\mu 2}^+)=0.0589\pm0.0021$. Using $K_{\pi 2}^+/K_{\mu 2}^+$ given above, we get $K_{e3}^+/K_{\mu 2}^+=0.0781\pm0.0029$. This determination was based on approximately 1700 observed events, and had very good positron identification. In order to cover a large momentum interval, the data were taken at three different magnetic fields and the normalization gave rise to a greater error than one would get based solely on the number of events. Since the two results come from independent measurements, we take for the weighted average $K_{e3}^+/K_{\mu 2}^+=0.0785\pm0.0025$.

The ratio $K_{\mu 3}^+/K_{\mu 2}^+$ cannot be evaluated directly from our measured numbers of $K_{\mu 3}^+$ and $K_{\mu 2}^+$ events because the fraction of the muon spectrum actually observed depends on the strong interaction form factors $f_+(q^2)$ and $f_-(q^2)$. If we assume vector coupling and make the approximation that $f_\pm(q^2)=f_\pm(0)$, the muon energy distribution is given by[4]

$$\frac{d\Gamma(E_\mu,\xi)}{dE_\mu}=\frac{\frac{1}{2}G^2|f_+(0)|^2}{2M_k(2\pi)^3}g(E_\mu)\{a(E_\mu)+2b(E_\mu)\,\mathrm{Re}\xi+c(E_\mu)[(\mathrm{Re}\xi)^2+(\mathrm{Im}\xi)^2]\},\quad(1)$$

where $\xi=f_-/f_+$, and the functions $a(E_\mu)$, $b(E_\mu)$, and $c(E_\mu)$ are independent of ξ. For what follows, it is a good approximation to set $\mathrm{Im}\xi=0$ so that we have, in addition to (1), the relation

$$(K_{\mu 3}^+/K_{e3}^+)_{\mathrm{theor}}=0.649+0.127(\mathrm{Re}\xi)+0.0193(\mathrm{Re}\xi)^2.\quad(2)$$

By writing

$$K_{\mu 3}^+/K_{e3}^+=(n_{\mu 3}/N_{e3})S(\xi),\quad(3)$$

where $n_{\mu 3}$ is the observed number of $K_{\mu 3}^+$ in the momentum interval 130 to 190 MeV/c, N_{e3} is the total number of K_{e3}^+ for this experiment and

$$S(\xi)=\int_0^{E_{\max}}d\Gamma(E_\mu,\xi)\Big/\int_{E_1}^{E_2}d\Gamma(E_\mu,\xi),$$

we can find the pair of solutions for ξ which satisfy (2) and (3) and get the corresponding branching ratios. A plot of Eqs. (2) and (3) is given in Fig. 10. The resulting two values of ξ are $+0.75\pm0.5$ and -5.4 ± 0.5.

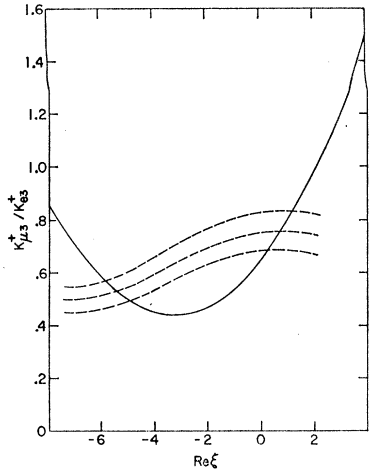

FIG. 10. The ratio of $K_{\mu 3}^+/K_{e3}^+$ as a function of Reξ. The parabolic curve is Eq. (2) of the text, the other curve is Eq. (3). The central dashed curve is the measured value and the upper and lower curves are one standard deviation from the central value.

Since our data are taken over the momentum interval from 130 to 190 MeV/c, our determination of ξ based on the shape of the $K_{\mu 3}^+$ spectrum is not good enough to enable us to choose between the values obtained from the branching-ratio analysis. Using the muon-polarization experiments[5] to rule out large negative values of ξ, we take $\xi=+0.75$, giving us a total of 834 ± 64 $K_{\mu 3}^+$ events for our experiment.[6] This yields a relative rate $K_{\mu 3}^+/K_{\mu 2}^+=0.0602\pm0.0046$.

The event totals $N_{\mu 2}$, $N_{\pi 2}$, N_{e3}, and $N_{\mu 3}$ obtained in this experiment, taken with the branching ratio (see Appendix A) $(\tau+\tau')=0.0728\pm0.0009$ can be used to determine the branching ratios for the modes $K_{\mu 2}^+$,

TABLE I. K^+ branching ratios determined in this experiment. The value given in Column 2 for K_{e3}^+ is the effective weighted mean for the two independent K_{e3}^+ measurements (see Ref. 1).

Mode	Totals used for branching ratios	Branching ratios
$K_{\mu 2}^+$	13 843±132	0.6334±0.0044
$K_{\pi 2}^+$	4501± 80	0.2059±0.0040
$K_{\mu 3}^+$	834± 64	0.0382±0.0029
K_{e3}^+	1086± 35	0.0497±0.0016

[4] N. Brene, L. Egardt, and B. Qvist, Nucl. Phys. **22**, 553 (1961); P. Dennery and H. Primakoff, Phys. Rev. **131**, 1334 (1963).

[5] V. Smirnitski and A. O. Weissenberg, Phys. Rev. Letters **12** 223 (1964); G. Borreani, G. Gidal, G. Rinaudo, A. E. Werbrouck, A. Carforio, C. M. Carelli, S. Natali, and M. Villani, Phys. Rev. **140**, B1686 (1965); and A. C. Callahan, V. Camerini, R. D. Hantman, R. H. March, D. L. Murphree, G. Gidal, G. E. Kalmus, W. M. Powell, C. L. Sandler, R. T. Pu, S. Natali, and M. Villani, Phys. Rev. (to be published).

[6] It should be emphasized that a variation in ξ from -1.0 to $+2.0$ produces a total change of less than 2.5% in $S(\xi)$, as is indicated in Fig. 10.

TABLE II. Summary of currently available measurements of the branching ratios $K_{\mu 2}^+$, $K_{\pi 2}^+$, K_{e3}^+, and $K_{\mu 3}^+$. Note that the values in rows 6–9 depend on the τ branching ratio; the values from this experiment depend on $[1-(\tau+\tau')]$.

References	Branching ratio % $K_{\mu 2}^+$	$K_{\pi 2}^+$	K_{e3}^+	$K_{\mu 3}^+$	Method; normalization
Birge[a]	58.5 ±3	27.7 ±2.7	3.2 ±1.3	2.8 ±1.0	Emulsion
Alexander[b]	56.9 ±2.6	23.2 ±2.2	5.1 ±1.3	5.9 ±1.3	Emulsion
Taylor[c]				2.8 ±0.4	Emulsion
Roe (Ref. 8)	64.2 ±1.3	18.6 ±0.9	5.0 ±0.5	4.8 ±0.6	Xenon bubble chamber
Shaklee (Ref. 9)	63.0 ±0.8	22.4 ±0.8	4.7 ±0.3	3.0 ±0.5	Xenon bubble chamber
Borreani[d]			5.12±0.36		Hydrogen bubble chamber; $\tau=5.7\%$
Bisi[e]				3.45±0.2	Hydrogen bubble chamber; $\tau=5.46\%$
Callahan[f]		21.0 ±0.56			Propane-freon bubble chamber Freon bubble chamber; $\tau=5.46\%$
Callahan (Ref. 5)		21.6 ±0.9	3.94±0.17	2.77±0.18	Freon bubble chamber; $\tau=5.46\%$
This experiment	63.34±0.44	20.59±0.40	4.97±0.16	3.82±0.29	Spark chamber; $(\tau+\tau')=7.27\%$

[a] R. W. Birge, D. H. Perkins, J. E. Peterson, D. H. Stork, and M. W. Whitehead, Nuovo Cimento **4**, 834 (1959).
[b] G. Alexander, R. H. W. Johnson, and C. O'Cealleigh, Nuovo Cimento **6**, 478 (1957).
[c] S. Taylor, G. Harris, J. Orear, J. Lee, and P. Baumel, Phys. Rev. **114**, 359 (1959).
[d] G. Borreani, G. Rinaudo, and A. E. Werbrouck, Phys. Letters **12**, 123 (1964).
[e] V. Bisi, G. Borreani, A. Marzari-Chiesa, G. Rinaudo, M. Vigone, and A. E. Werbrouck, Phys. Rev. **139**, B1068 (1965).
[f] A. Callahan and D. Cline, Phys. Rev. Letters **15**, 129 (1965).

$K_{\mu 2}^+$, K_{e3}^+, and $K_{\mu 3}^+$. Let

$$N_0=N_{\mu 2}+N_{\pi 2}+N_{e3}+N_{\mu 3}.$$

The effective number of decaying K^+ for this experiment is then

$$N_{\text{total}}=N_0/[1-(\tau+\tau')],$$

and the branching ratio into the jth mode is

$$K_j^+=N_j/N_{\text{total}}.$$

We present in Table I the branching ratios for $K_{\mu 2}^+$, $K_{\pi 2}^+$, K_{e3}^+, and $K_{\mu 3}^+$, which are the basic results of this paper. The K_{e3}^+ branching ratio listed in the table is the weighted average of the value obtained using the range chamber, (5.04±0.33)% with the value obtained using the Čherenkov counter, (4.94±0.18)%.

V. CONCLUSIONS

In Table II we present all the published data known to us pertaining to the four decay modes studied in this experiment. As can be seen, some of the values listed differ from one another by considerably more than the quoted errors. The discrepancies in the $K_{\mu 3}^+$ and $K_{\pi 2}^+$ numbers are particularly serious, presumably indicating the presence of systematic errors.

Much of the inconsistency can be removed, however, by using measured quantities which are less subject to systematic errors than the quoted final branching ratios. In particular, it is difficult in a xenon bubble chamber[7] to separate the $K_{\pi 2}^+$ and $K_{\mu 3}^+$ modes, so that we use the sum of these modes from Roe *et al.*,[8] and from Shaklee *et al.*[9] Further, Callahan *et al.*[5] make a careful measurement, using a sample of their data, of the $K_{\mu 3}^+$ to K_{e3}^+ ratio, which we use. Independently, an absolute normalization is also quoted[10] which gives a K_{e3}^+ rate that is in strong disagreement with other data. The branching ratios based on that normalization are therefore rejected from our compilation. In Appendix B we list all of the selected data and describe the averaging technique used to obtain what we consider to be the best weighted average values for the K^+ branching ratios. These weighted averages are given in Table III.

From the value of $K_{\mu 3}^+/K_{e3}^+$ given in Table III one gets for Reξ the values -7.15 ± 0.20 and $+0.57\pm0.20$, where it is assumed that Im$\xi=0$ and that there is no energy dependence of the form factors.

The rate $\Gamma(K_{e3}^+)=(3.96\pm0.11)\times10^6$ sec^{-1} yields for the Cabibbo angle[10] for the polar-vector component of the weak interaction current, $\theta_V=0.222\pm0.008$, allowing a reasonable variation[11] of $f_+(q^2)$ with q^2. Radiative

TABLE III. Weighted averages of the K^+ branching ratios from the input data given in Appendix B.

Decay mode	Branching ratio (weighted average) (%)
$K_{\mu 2}^+$	63.34 ±0.37
$K_{\pi 2}^+$	20.96 ±0.29
K_{e3}^+	4.93 ±0.13
$K_{\mu 3}^+$	3.59 ±0.14
τ	5.58 ±0.08
τ'	1.69 ±0.05
$K_{\mu 3}^+/K_{e3}^+$	0.721±0.031

[7] B. P. Roe (private communication).
[8] B. P. Roe, D. Sinclair, J. L. Brown, D. Glasser, J. A. Kadyk, and G. H. Trilling, Phys. Rev. Letters **7**, 346 (1961).
[9] F. S. Shaklee, G. L. Jensen, B. P. Roe, and D. Sinclair, Phys. Rev. **136**, B1423 (1964).
[10] N. Cabibbo, Phys. Rev. Letters **10**, 531 (1963), and N. Cabibbo, in Proceedings of the 13th International Conference on High-Energy Physics, Berkeley, California, 1966 (unpublished). Cabibbo, in his rapporteur's talk at the above conference, gave the result of a calculation for $\Gamma(K_{e3}^+)$ as $\Gamma(K_{e3}^+)=\sin^2\theta[2f_+^2(0)]\times[1+0.277(M_K/M_+)^2]\times[7.42\times10^7]$ sec^{-1}. Determinations of M_+ lie in the range 700 MeV to infinity. We have used for the K^+ lifetime the value $(1.243\pm0.004)\times10^{-8}$ sec, and for M_+ the value 890 MeV.
[11] S. Oneda and J. Sucher, Phys. Rev. Letters **15**, 927, 1049(E) (1965).

effects,[12] and symmetry-breaking effects[13,14] may well be several percent. The corresponding angle obtained from nuclear beta-decay measurements, $\theta_V{}^\beta$, is known[15] to have the value $\theta_V{}^\beta=0.210\pm0.005$, where the error is experimental. It has, however, been pointed out[16] that uncertainties in the radiative corrections necessary to obtain $\theta_V{}^\beta$ may be as large as about 10%. Hence within the uncertainties of the theoretical corrections there is no disagreement between θ_V and $\theta_V{}^\beta$. Our value of $\Gamma(K_{\mu2}{}^+)=(50.96\pm0.34)\times10^6$ sec^{-1} gives the axial-vector angle as $\theta_A=0.2646\pm0.0015$, again without corrections. The difference between θ_V and θ_A has been the subject of a number of recent theoretical investigations of first-order symmetry-breaking effects.[17]

The leptonic $|\Delta\mathbf{I}|=\frac{1}{2}$ rule requires that

$$\Gamma_L(\text{lept})\equiv\Gamma[(K_L{}^0\to\pi^\pm+\mu^\mp+\nu)+(K_L{}^0\to\pi^\pm+e^\mp+\nu)]$$
$$=2\Gamma_+(\text{lept})\equiv2\Gamma[(K^+\to\pi^0+\mu^+\nu)+(K^+\to\pi^0+e^+\nu)].$$

The best fit to $K_L{}^0$ data,[18] which includes lifetime measurements and measurements of relative and absolute decay rates, yields $\Gamma_L(\text{lept})=(12.80\pm0.64)\times10^6$ sec^{-1}. Using the values of $\Gamma(K_{e3}{}^+)$ and $\Gamma(K_{\mu3}{}^+)$ given in Table III, we obtain $2\Gamma_+(\text{lept})=(13.72\pm0.31)\times10^6$ sec^{-1}, so that

$$\Gamma_L(\text{lept})/2\Gamma_+(\text{lept})=0.933\pm0.051,$$

which is in agreement with the leptonic $|\Delta\mathbf{I}|=\frac{1}{2}$ rule.

ACKNOWLEDGMENTS

We would like to thank the Princeton-Pennsylvania Accelerator operating staff for their efforts on our behalf and for their unfailing cooperation. K. E. Wright and his staff were responsible for the mechanical design and construction of much of the apparatus, and H. Crothamel, B. Gibbs, and E. Mayer for most of the electronics construction. We also acknowledge the help of R. Imlay and D. Bowen in running the experiment. We are indebted to D. Bowen and Dr. A. Franklin for their assistance with the electron range distributions. We are grateful to the film measuring staff, under Mrs. Y. Kim and Miss S. Markowitch who performed enthusiastically and concientiously. All of the calculations were carried out at the Princeton computer center.

[12] E. S. Ginsberg, Phys. Rev. **142**, 1035 (1966).
[13] M. Ademollo and R. Gatto, Phys. Rev. Letters **13**, 264 (1964); H. T. Nieh, *ibid.* **15**, 902 (1965).
[14] G. Furlan, F. G. Lannoy, C. Rossetti, and G. Segrè, Nuovo Cimento **38**, 1747 (1965).
[15] C. S. Wu, Rev. Mod. Phys. **36**, 618 (1964); Joan M. Freeman, J. G. Jenkin, G. Murray, and W. E. Burcham, in Proceedings of the International Conference on Weak Interactions, 1965, p. 327 (unpublished); Phys. Rev. Letters **16**, 959 (1966).
[16] S. M. Berman and A. Sirlin, Ann. Phys. (N.Y.) **20**, 20 (1962); A. Sirlin, Phys. Rev. Letters **16**, 872 (1966).
[17] R. Oehme, Phys. Rev. Letters **12**, 550 (1964); R. Oehme and G. Segrè, Phys. Letters **11**, 94 (1964); R. Oehme, Ann. Phys. (N. Y.) **33**, 108 (1965); C. G. Callan and S. B. Treiman, Phys. Rev. Letters **16**, 153 (1966). M. Suzuki, *ibid.* **16**, 212 (1965); R. Oehme, *ibid.* **16**, 215 (1965); V. S. Mathur, S. Okubo, and L. K. Pandit, *ibid.* **16**, 371 (1965).
[18] T. Devlin (private communication). Dr. Devlin, using his recently measured $K_2{}^0$ lifetime in combination with published data has calculated $\Gamma(K_L{}^0\to\pi^\pm+e^+\nu)$ and $\Gamma(K_L{}^0\to\pi^\pm+\mu^\mp+\nu)$.

APPENDIX A

Listed in Table IV are all the values of the τ and τ' branching ratios measured in experiments having more than 100 events. The values agree quite well except for

TABLE IV. Summary of τ and τ' branching ratio values.

Reference \ Decay mode	$K^+\to\pi^++\pi^++\pi^-$ (τ)	$K^+\to\pi^++\pi^0+\pi^0$ (τ')
Birge[a]	5.6 ±0.4	2.1±0.5
Alexander[b]	6.8 ±0.4	2.2±0.4
Taylor[c]	5.2 ±0.3	1.5±0.2
Roe (Ref. 8)	5.7 ±0.3	1.7±0.2
Shaklee (Ref. 9)	5.1 ±0.2	1.8±0.2
Callahan[d]	5.54±0.12	
Demarco-Trabuco[e]	5.71±0.15	
Bisi (Ref. 19)	$\tau'/\tau=0.303\pm0.009$	

[a] See footnote a of Table II.
[b] See footnote b of Table II.
[c] See footnote c of Table II.
[d] A. Callahan, R. March, and R. Stark, Phys. Rev. **136**, B1463 (1964).
[e] A. DeMarco-Trabuco, C. Brosso, and G. Rinaudo, Phys. Rev. **140**, B1430 (1965).

entries 2 and 5. The average of all these data (weighting them by the square of the quoted errors) is (5.56 ±0.08)% with a χ^2 probability of less than one percent. If we exclude both 2 and 5 the average is (5.58±0.08)% with a χ^2 probability of 62%. We take this to be the best value.

Using (5.58±0.08)% for the τ branching ratio, and the τ'/τ ratio of Bisi *et al.*,[19] we obtain $\tau'=(1.69\pm0.055)\%$. The weighted average of this with other measurements of the τ' branching ratio is (1.70 ±0.05)%, giving (7.28±0.09)% as the sum of τ and τ'.

APPENDIX B

The selected experimental values (renormalized to a consistent value of the τ branching ratio, i.e., 5.58%)

TABLE V. Selected measurements of K^+ decay relative rates used as input data for the results of Table III.

Mode	Reference	Branching ratio (%)
$K_{\mu2}{}^+$	Roe (Ref. 8)	64.2 ±1.3
	Shaklee (Ref. 9)	63.0 ±0.8
	This expt.	63.34 ±0.44
$K_{\pi2}{}^+$	Callahan[a]	21.46 ±0.56
	This expt.	20.59 ±0.40
$K_{e3}{}^+$	Roe (Ref. 8)	5.0 ±0.5
	Shaklee (Ref. 9)	4.7 ±0.3
	Borreani[b]	5.01 ±0.35
	This expt.	4.97 ±0.16
$K_{\mu3}{}^+$	Bisi[c]	3.53 ±0.20
	This expt.	3.82 ±0.29
$K_{\mu3}{}^+/K_{e3}$	Callahan (Ref. 5)	0.703±0.056
$K_{\pi2}{}^++K_{\mu3}{}^+$	Roe (Ref. 8)	23.4 ±1.1
	Shaklee (Ref. 9)	25.4 ±0.7

[a] See footnote f of Table II.
[b] See footnote d of Table II.
[c] See footnote e of Table II.

[19] V. Bisi, G. Borreani, R. Cester, A. DeMarco-Trabuco, M. I. Ferrero, C. M. Garrelli, A. Marzari Chiesa, B. Quassiatti, G. Rinaudo, M. Vigone, and A. E. Werbrouck, Nuovo Cimento **35**, 768 (1965).

used to obtain our weighted averages are listed in Table V. For the reasons given earlier, we have excluded the emulsion data. The weighted average of the four values listed in Table V for the K_{e3}^+ branching ratio is $(4.93\pm0.13)\%$. Using this value and the $K_{\mu3}^+/K_{e3}^+$ ratio from Callahan *et al.*,[5] one obtains a $K_{\mu3}^+$ branching ratio of $(3.47\pm0.29)\%$. Combining this latter value with the two values listed in Table V, our weighted average for the $K_{\mu3}^+$ branching ratio is $(3.59\pm0.14)\%$. Subtracting this from the $(K_{\pi2}^+ + K_{\mu3}^+)$ entries and averaging the resultant $K_{\pi2}^+$ values with those listed in Table V, we get a best value for the $K_{\pi2}^+$ branching ratio of $(20.96\pm0.29)\%$. A straightforward weighted average of the $K_{\mu2}^+$ data yields $(63.34\pm0.37)\%$. The sum of the branching ratios given above with the value assumed for $\tau+\tau'$ is 100.09, making readjustment unnecessary. To determine the relative rate $K_{\mu3}^+/K_{e3}^+$, we have divided the weighted average of the $K_{\mu3}^+$ entries in Table V by that of the K_{e3}^+ entries and taken the weighted average of that number with the $K_{\mu3}^+/K_{e3}^+$ value of Callahan *et al.*,[5] obtaining 0.721 ± 0.031.

PHYSICAL REVIEW VOLUME 155, NUMBER 5 25 MARCH 1967

Some Remarks on the Kinematic Singularities of the Helicity Amplitudes

KEH YING LIN*
Laboratory of Nuclear Studies, Cornell University, Ithaca, New York
(Received 7 November 1966)

The question of whether the kinematic singularities at $t=0$ of the t-channel helicity amplitudes are relevant to the behavior of the differential cross section at high energy and small momentum transfer has been examined. It is concluded that they can be ignored in the phenomenological analysis of two-particle reactions.

I. INTRODUCTION

RECENTLY, experimental study of the reactions p (proton)$+p\rightarrow p+N^*$ has indicated that the corresponding differential cross sections at high energy and small momentum transfer (between protons) show, in general, a sharp dropoff.[1] The differential cross section can be expressed in terms of either the direct-channel helicity amplitudes or, by means of the crossing relations, the crossed-channel helicity amplitudes. Recently, a method to identify the kinematic singularities of the helicity amplitudes was proposed, using the Trueman-Wick crossing relations.[2] According to this method, one would expect that the crossed-channel helicity amplitudes possess kinematic singularities at the following positions: $t=0$, $4M^2$, and $(M^*\pm M)^2$, where t is the squared momentum transfer, and M and M^* are the masses of the proton and the resonance, respectively. More precisely, the differential cross section, when expressed in terms of the t-channel helicity amplitudes, behaves like t^{-1} near $t=0$. This prediction cannot be checked by experiment because t is always negative in the physical region of the direct channel. However, at very high energy we have $|t|_{\min}\approx M^2(M^{*2}-M^2)^2s^{-2}$, where $|t|_{\min}$ means the smallest value of $|t|$ in the physical region of the direct channel, and s is the total energy square in the c.m. system. Notice that $|t|_{\min}$ can be as close to zero as possible by pushing s high enough. It is natural to ask whether the behavior of the differential cross section or the residue functions of the Regge trajectories[3] at high energy and small momentum transfer in the physical region is closely related to the kinematic singularities at $t=0$.

This problem does not occur in the case of elastic scattering, where $t=0$ corresponds to the forward scattering. It only occurs in the case of $a+b\rightarrow c+d$, where particles a and c have the same mass, b and d have different masses, and t is the squared 4-momentum transfer between a and c. In this case, the differential cross section, in terms of the t-channel helicity amplitudes, behaves like $t^{-J(a)-J(c)}$ near $t=0$, where $J(a)$ means the spin of a.

We have examined this problem and have found that the kinematic singularities of the t-channel helicity amplitudes at $t=0$ can be ignored in any phenomenological analysis of the two-particle interactions. In order to make this paper more or less self-consistent, we shall describe briefly the method to identify the kinematic singularities in Sec. II. We shall present our arguments in Sec. III.

II. THE METHOD TO IDENTIFY THE KINEMATIC SINGULARITIES OF THE DIRECT-CHANNEL HELICITY AMPLITUDES

We shall review briefly the method used in Ref. 2. Let us consider the reaction $a+b\rightarrow c+d$. The s-channel

* Supported in part by the U. S. Office of Naval Research.
[1] E. W. Anderson *et al.*, Phys. Rev. Letters **16**, 855 (1966).
[2] L. L. C. Wang, Phys. Rev. **142**, 1187 (1966).
[3] E. Leader, Rev. Mod. Phys. **38**, 476 (1966).